Supporting Information

Ultrathin δ-MnO_2 nanoflakes with Na^+ intercalation as a high-capacity cathode for aqueous zinc-ion battery

Haijun Peng[a], Huiqing Fan[a,*], Chenhui Yang[b], Yapeng Tian[c], Chao Wang[a], Jianan Sui[a]

[a] State Key Laboratory of Solidification Processing, School of Materials Science and Engineering, Northwestern Polytechnical University, Xi'an 710072, China
[b] School of Natural and Applied Sciences, Northwestern Polytechnical University, Xi'an 710072, China
[c] Electronic Materials Research Laboratory, International Center for Dielectric Research, Key Laboratory of the Ministry of Education, School of Electronic & Information Engineering, Xi'an Jiaotong University, Xi'an 710049, China

Corresponding author. **E-mail:** hqfan@nwpu.edu.cn; hqfan3@163.com

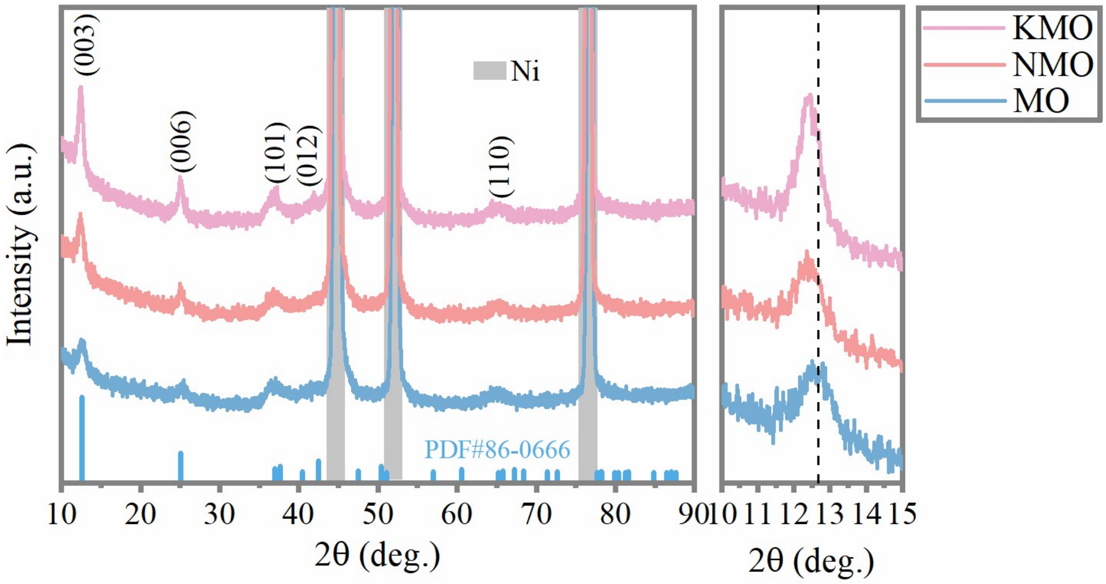

Figure S1. XRD patterns of the MO (after K-ion extraction), NMO and KMO nanoflakes.

It can be observed that the (003) peaks belonging to the NMO and KMO samples show negative shift comparing to that of the MO, which indicates the enhanced interlayer spacing attributed to the Na^+ and K^+ intercalation into the host layer of δ-MnO_2.

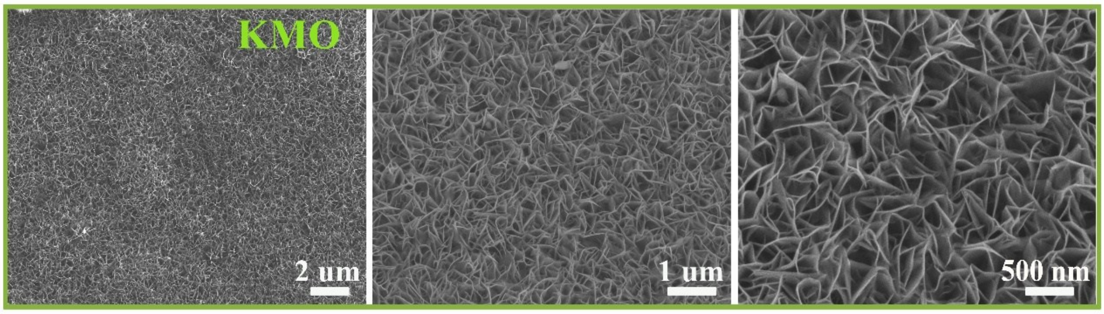

Figure S2. SEM images of KMO nanoflakes.

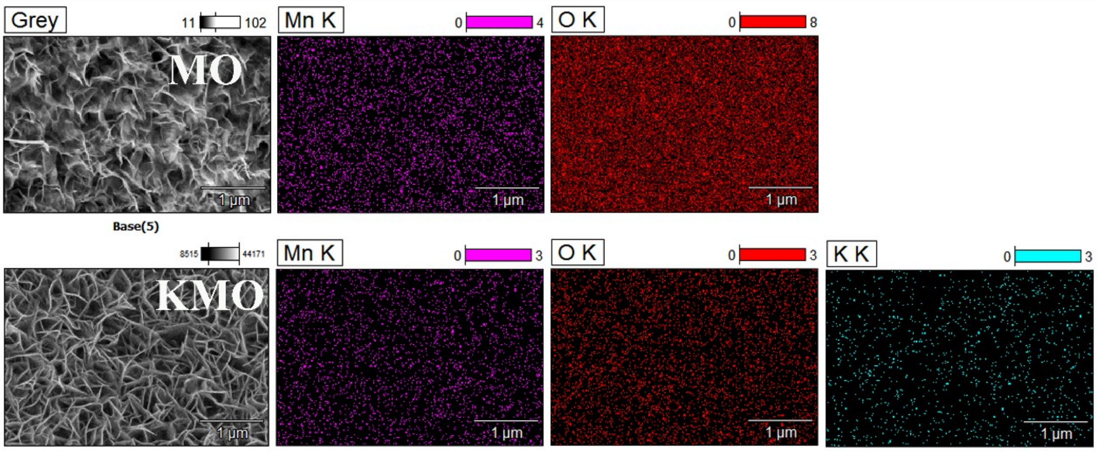

Figure S3. SEM and EDX element mapping images of the MO and KMO samples.

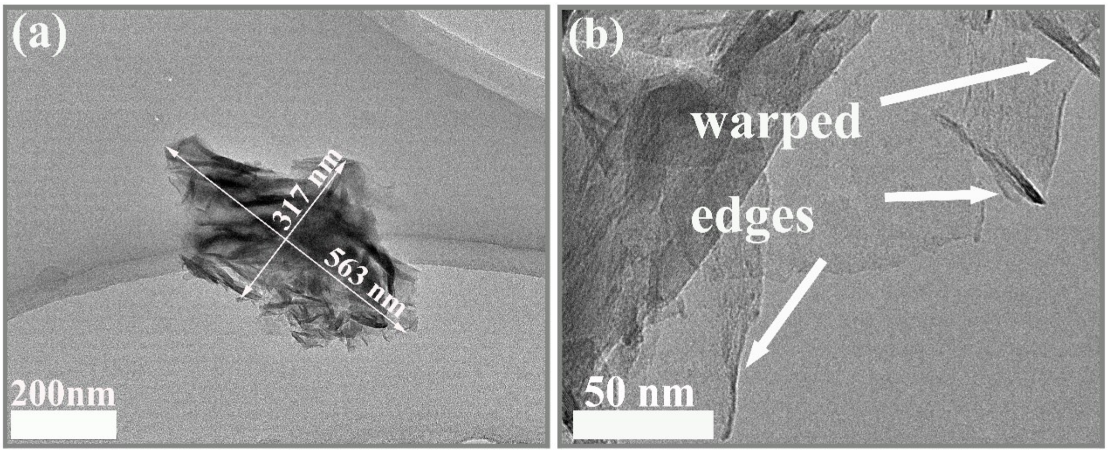

Figure S4. TEM images of NMO nanoflakes.

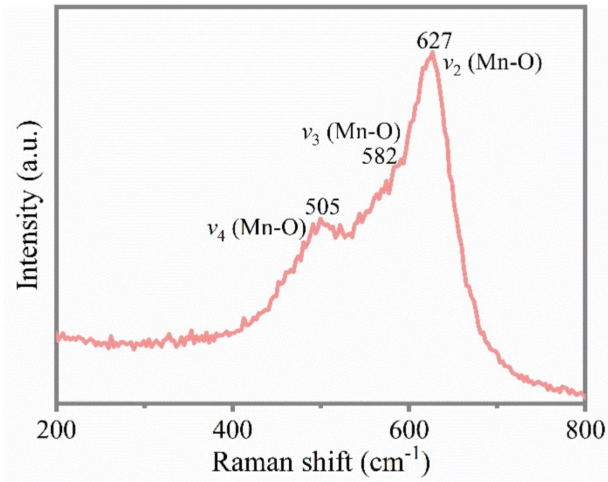

Figure S5. Raman spectrum of NMO nanoflakes.

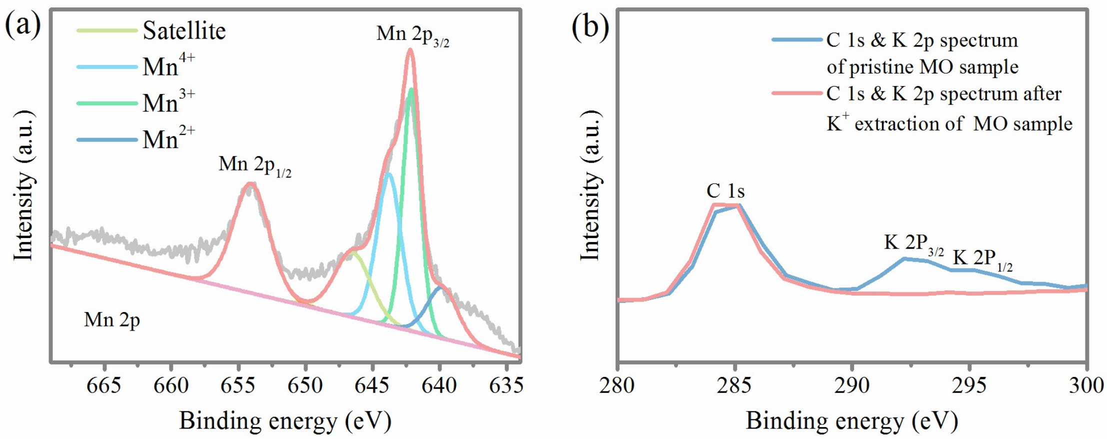

Figure S6. High-resolution XPS spectra of (a) Mn 2p of NMO nanoflakes, and (b) C 1s and K 2p of pristine δ-MnO_2 and after K^+ ion extraction of δ-MnO_2 nanoflakes.

The vanishment of K $2p_{3/2}$ and K $2p_{1/2}$ peaks in Figure S5b verified the successful K^+ ion extraction from pristine δ-MnO_2 sample. The average oxidation state of Mn in the as-prepared MnO_2 is calculated according to the following equation [1]:

$$AOS = 8.95 - 1.13\Delta E \text{ (eV)} \quad \text{(S1)}$$

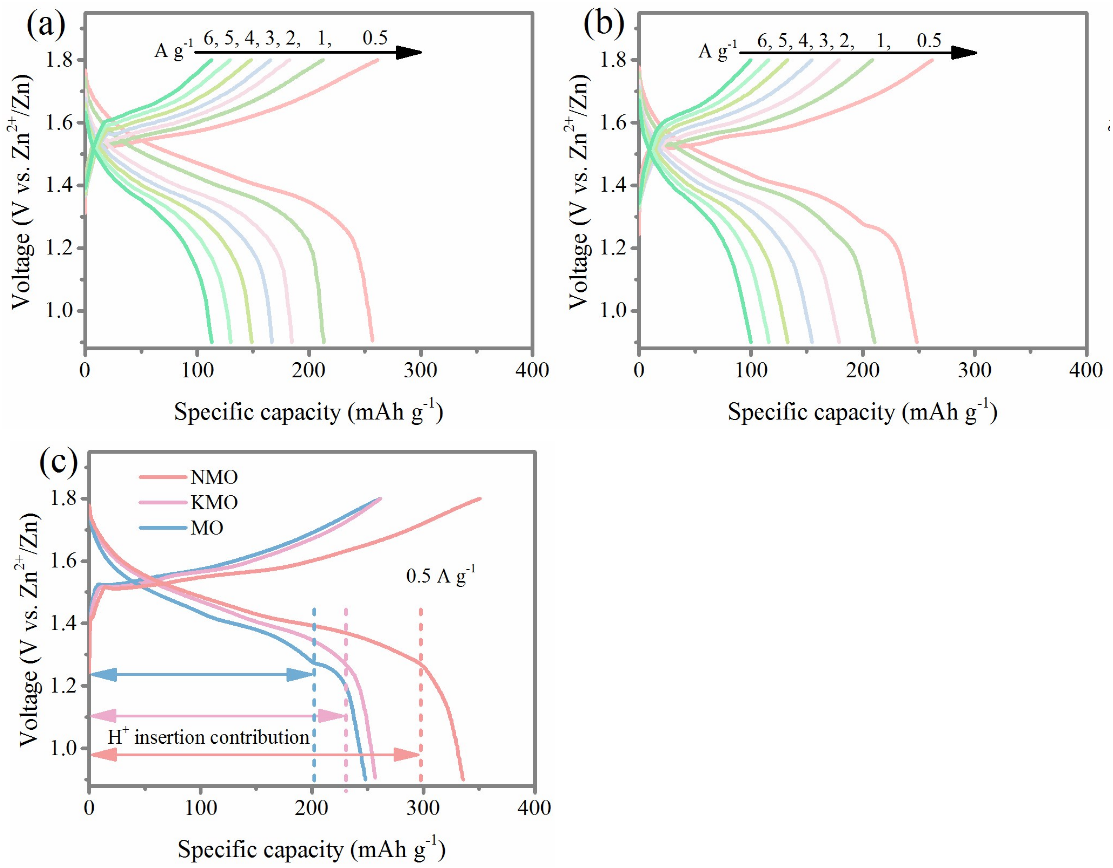

Figure S7. Charge/discharge profiles at different current densities varying from 0.5 to 6 A g^{-1} of the Zn/KMO (a) and Zn/MO (b) batteries. (c) The plots of three batteries under the current density of 0.5 A g^{-1}.

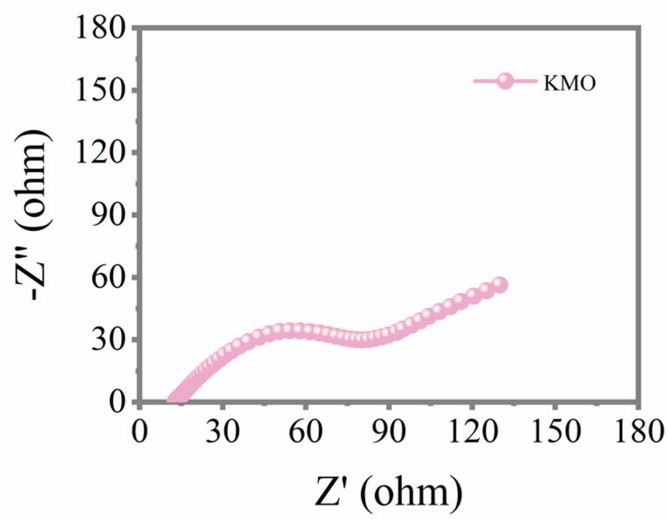

Figure S8. Nyquist plot of the Zn/KMO battery.

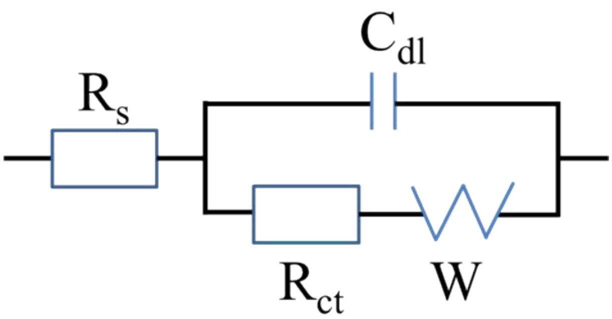

Figure S9. The equivalent circuit applied for simulation of EIS results based on Nyquist plots of the four batteries. (R_s: internal resistance of electrode, C_{dl}: electrical double layer capacitor, R_{ct}: charge transfer resistance, W: Warburg impedance).

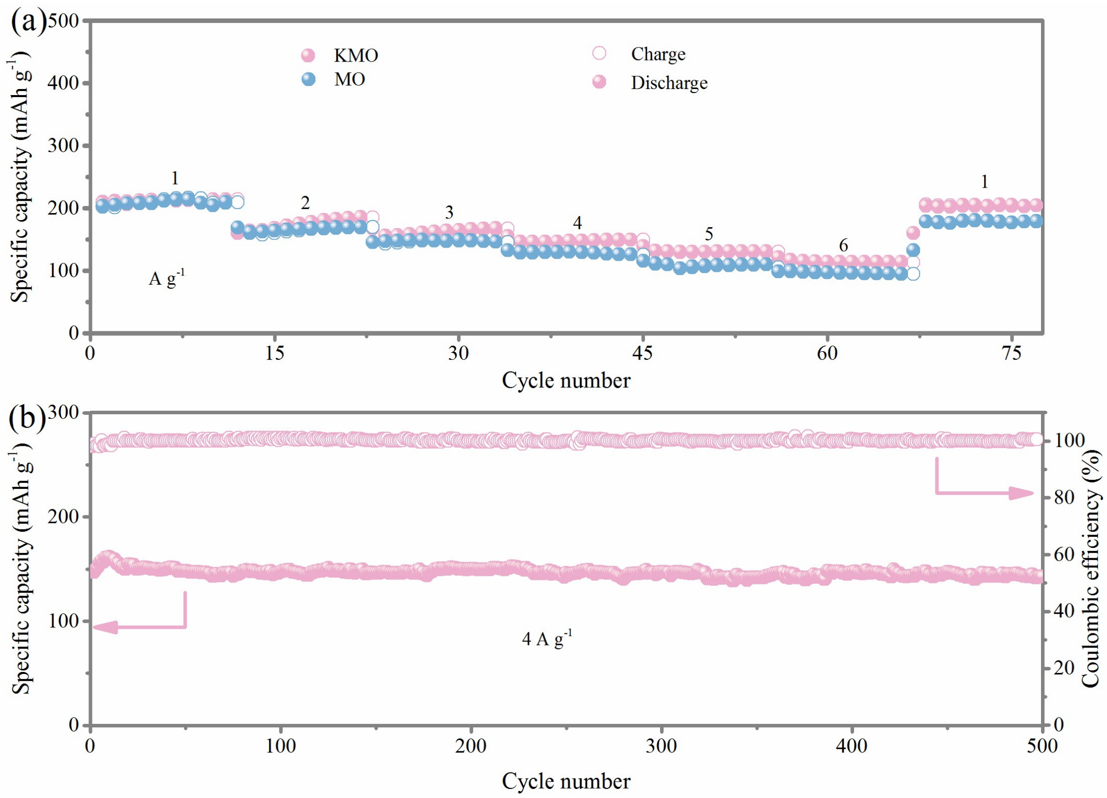

Figure S10. (a) Rate capability of the Zn/KMO and Zn/MO. (b) Long-life cycling performance of the Zn/KMO at different current densities.

The long-cycle performance of the Zn/KMO battery is evaluated at the current density of 4 A g^{-1}, which confirms the superior stability of the battery with 97.4% capacity retention. Interestingly, although the inferior specific capacity of the Zn/KMO to the Zn/NMO battery, the rate performance and long-term stability of the former are a little superior to the latter which may be attributed to the alleviated Mn dissolution suppressed by the inserted K^+ as the K^+ ions steadily intercalated into the interlayer of KMO and bonded with the Mn polyhedrons [2], indicating the more stability of the Zn/KMO battery in practice application.

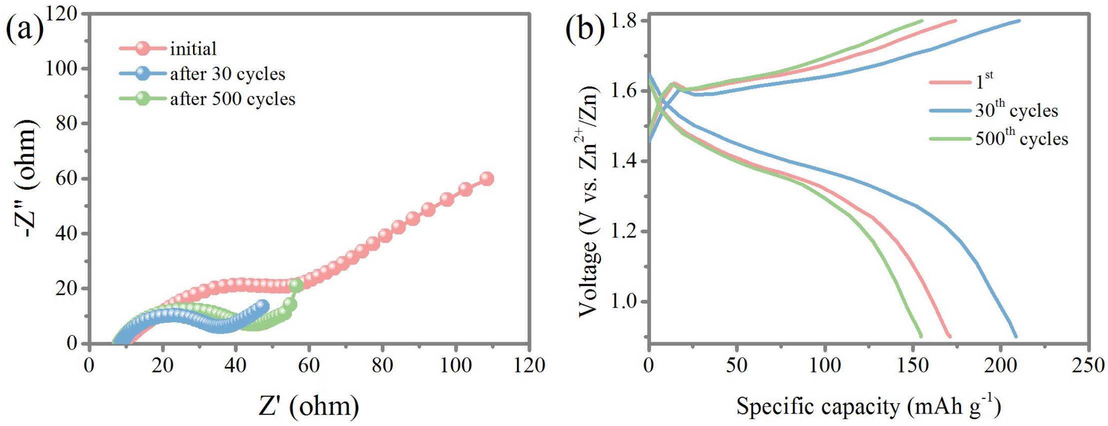

Figure S11. Nyquist plots (a) and XRD patterns (b) of Zn/NMO battery with different states under various cycles.

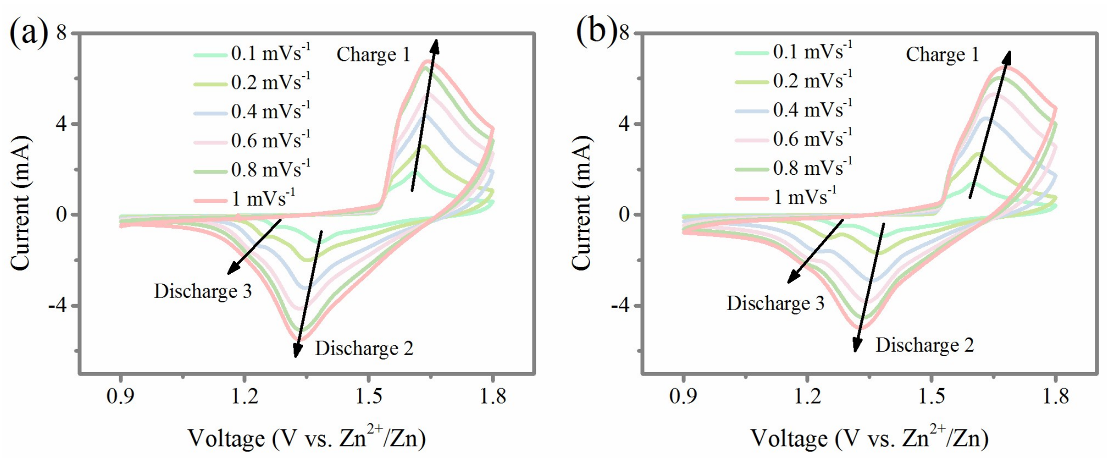

Figure S12. CV curves of the KMO (a) and MO (b) electrodes at different scan rates.

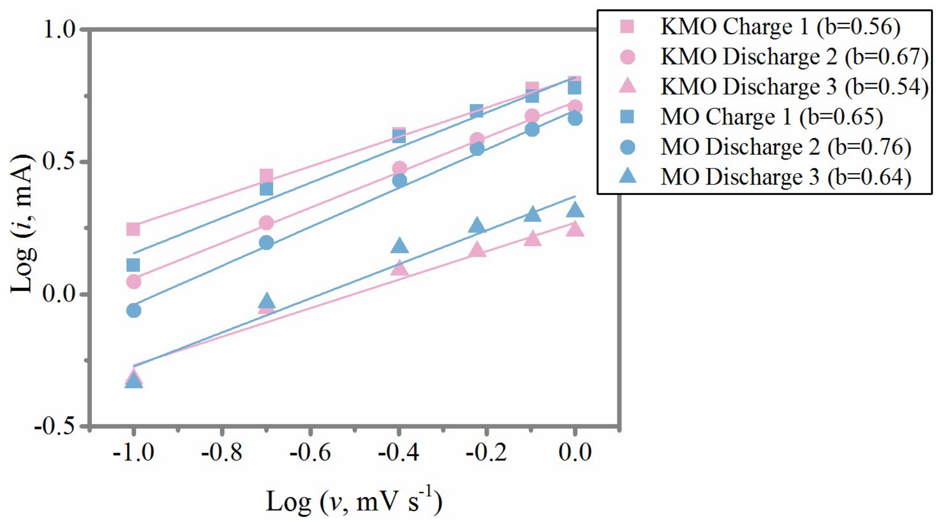

Figure S13. Log (i) vs. log (v) plots of the three peaks in CV curves for the KMO and MO cathodes.

Figure S14. Capacity contributions from diffusion-controlled and capacitive processes for the NMO (a), KMO (b), and MO (c) cathodes.

The investigation of the electrochemical kinetics was conducted in the basis of various CV scans rates between 0.1-1 mV s^{-1} for the three batteries as shown in Figure S12, S13 and S14. The peak currents (i) and the corresponding scan rates (v) coincide with the following Equations [3, 4]:

$$i = av^{b} \tag{S2}$$

$$\log i = \log a + b\log v \tag{S3}$$

Through calculating the slope of log i vs. log v linear regression lines, the value of coefficient b for peaks 1, 2 and 3 in the four batteries range from 0.55～0.76 (Figure S14). The calculation results imply that the electrochemical reaction of four batteries are mainly dominated by ionic diffusion process, instead of the kinetic characteristic controlled by the surface capacitive process within the scanning rate ranging from 0.1 to 1 mV s^{-1}. At the sametime, the percentage of capacitive contribution can be quantitatively analyzed via the following equations [5]:

$$i = k_1 v + k_2 v^{1/2} \tag{S4}$$

$$i/v^{1/2} = k_1 v^{1/2} + k_2 \tag{S5}$$

where i, $k_1 v$ and $k_2 v^{1/2}$ represent the total current response at a given potential corresponding to the three peaks in CV curves, the capacitive contribution and diffusion-controlled contribution, respectively. The values of k_1 and k_2 are determined by the employed plots of $i/v^{1/2}$ versus $v^{1/2}$. Apparently, the preinserted alkali cations (Na^+ and K^+) provide an improved diffusion-controlled contribution effect especially under the scan rates of 0.4-1 mV s^{-1} comparing to that of pristine δ-MnO_2 (MO) cathode (Figure S14). This is attributed to the enhanced ion conductivity caused by *in situ* introduction of alkali cations (Na^+ and K^+).

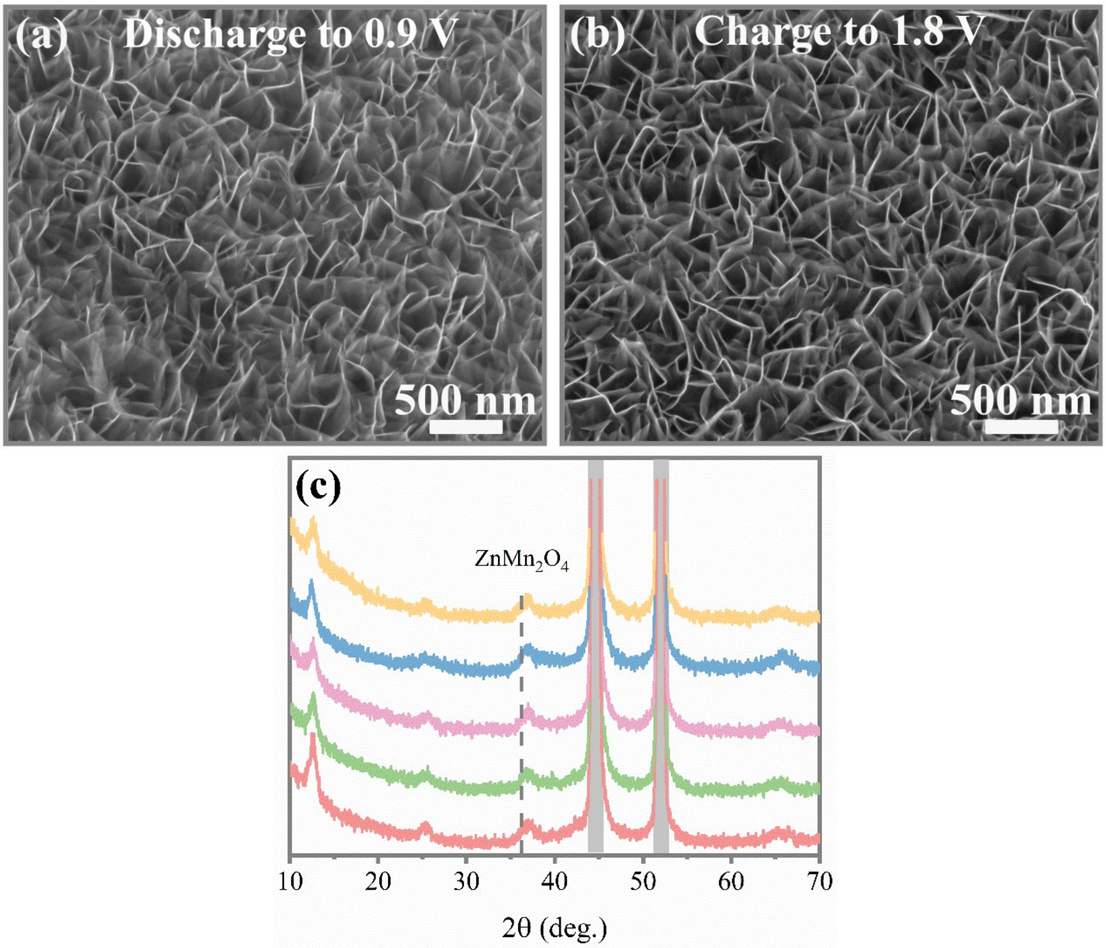

Figure S15. SEM images of NMO nanoflakes at discharge to 0.9 V (a) and charge to 1.8 V (b). (c) *Ex-situ* XRD patterns of at the selected potential states.

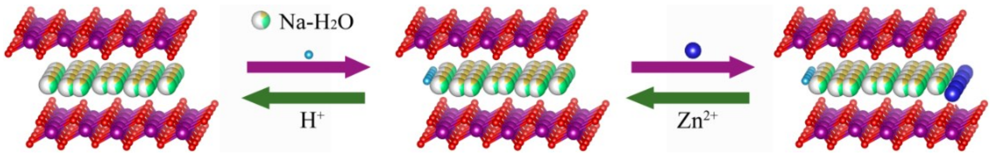

Figure S16. Schematic of the charge/discharge process of the involved sequential intercalation of H^+ and Zn^{2+} into the layered of the NMO cathode.

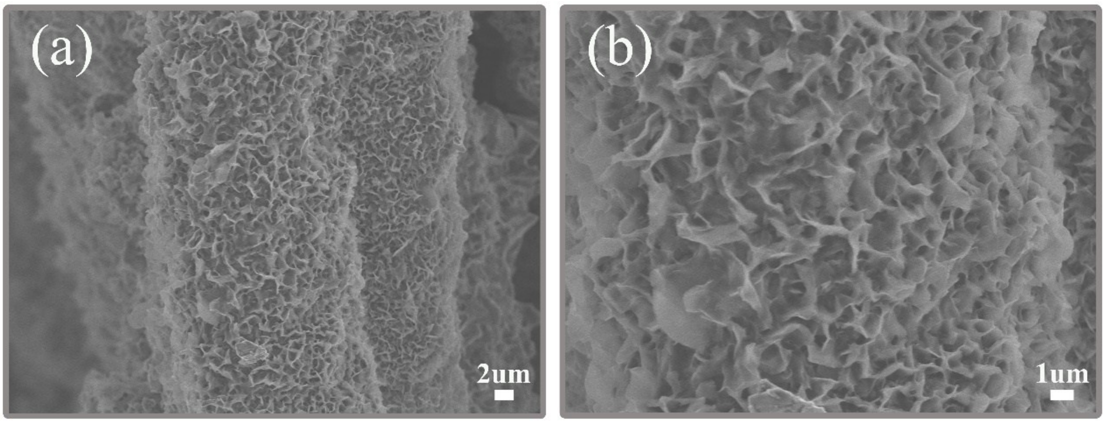

Figure S17. SEM images of the electrodeposition Zn nanoflakes under different magnifications.

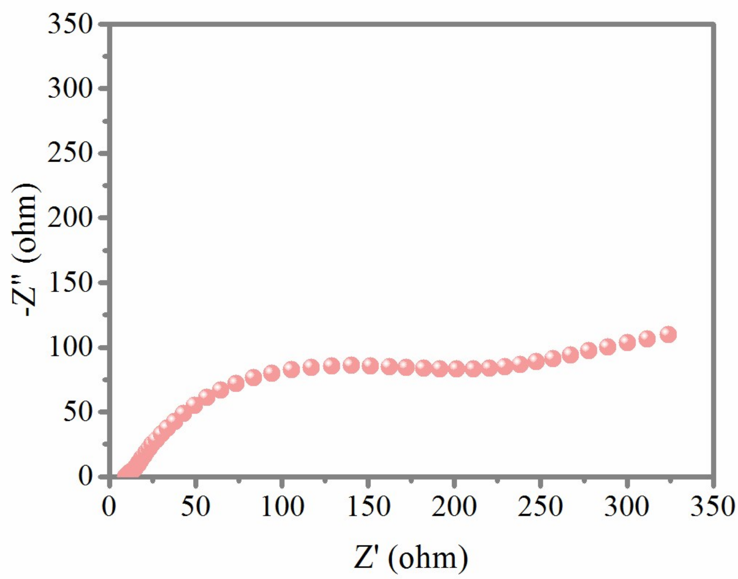

Figure S18. Nyquist plot of the Zn/NMO battery in polymer electrolyte.

Table S1. Elemental analysis of NMO nanoflakes by inductively coupled plasma optical emission spectroscopy (ICP-OES).

Sample	Na (wt%)	Mn (wt%)
1#	6.82	89.8
2#	6.77	89.5
3#	6.80	89.9

Table S2. The simulation results for EIS based on Nyquist plots of the three batteries.

Batteries	R_s (ohm)	R_{ct} (ohm)
Zn/MO	9.55	104.65
Zn/NMO	8.51	45.32
Zn/KMO	12.8	69.85

Table S3. Summary comparison for electrochemical performances of the NMO cathode with reported cathode materials in zinc-ion batteries.

Cathode	Electrolytes	Specific Capacity	Rate performance	Capacity retention	Reference
NMO	**2 M $ZnSO_4$ + 0.2 M $MnSO_4$**	**335 mA h g^{-1} at 0.5 A g^{-1}**	**39.1% retained at 6 A g^{-1}**	**93% after 1000 cycles at 4 A g^{-1}**	**This work**
MnO_2@PEDOT	PVA+3M LiCl+2 M $ZnCl_2$+0.4 M $MnSO_4$	366.6 mA h g-1 at 0.74 A g^{-1}	39.1% retained at 7.43 A g^{-1}	83.7% after 300 cycles at 1.11 A g^{-1}	[6]
O_d-MnO_2	1 M $ZnSO_4$ + 0.2 M $MnSO_4$	345 mAh g^{-1} at 0.2 A g^{-1}	～30% retained at 30 A g^{-1}	84% after 2000 cycles at 5 A g^{-1}	[7]
δ-MnO_2	1M $ZnSO_4$	252 mAh g^{-1} at 83 mA g^{-1}	24.6% retained at 1.33 A g^{-1}	44% after 100 cycles at 83 mA g^{-1}	[8]
α-MnO_2	1M $ZnSO_4$	353 mAh g^{-1} at 16 mA g^{-1}	12.2% retained at 1.33 A g^{-1}	63% after 50 cycles at 83 mA g^{-1}	[9]
β-MnO_2	3M $Zn(CF_3SO_3)_2$ + 0.1M $Mn(CF_3S_3)_2$	258 mAh g^{-1} at 0.65 C	38.8% retained at 32.50 C	94% after 2000 cycles at 6.50 C	[10]
Polyaniline-intercalated MnO_2	2M $ZnSO_4$ + 0.1 M $MnSO_4$	280 mA h g^{-1} at 200 mA g^{-1}	39.3% retained at 3 A g^{-1}	～100% after 200 cycles	[11]
$ZnMn_2O_4$@PEDOT	1 M $ZnSO_4$	207 mAh g^{-1} at 80 mA g^{-1}	67.6% retained at 1.613 A g^{-1}	93.8% retained after 300 cycles at 1.29 A g^{-1}	[12]
Layered MnO_2	1 M $ZnSO_4$	289 mAh g^{-1} at 50 mA g^{-1}	21.1% retained at 1 A g^{-1}	35% retained after 50 cycles at 0.1 A g^{-1}	[13]
MnO_x@ N-doped C	2 M $ZnSO_4$ + 0.1 M $MnSO_4$	385 mAh g^{-1} at 100 mA g^{-1}	31.9% retained at 2 A g^{-1}	99% retained after 1600 cycles at 2 A g^{-1}	[14]
MnO_2/rGO	2 M ZnSO4 + 0.1 M $MnSO_4$	332 mAh g^{-1} at 300 mA g^{-1}	51.8% retained at 6 A g^{-1}	96% retained after 500 cycles at 6 A g^{-1}	[15]
α-MnO_2 on 3D N-doped CC	2 M $ZnCl_2$ +0.4 M $MnSO_4$	353 mAh g^{-1} at 500 mA g^{-1}	70.5% retained at 6 A g^{-1}	94% retained after 1000 cycles at 1 A g^{-1}	[16]
α-MnO_2@graphene	2 M $ZnSO_4$ +0.2 M $MnSO_4$	382 mAh g^{-1} at 300 mA g^{-1}	55% retained at 3A g^{-1}	94% retained after 3000 cycles at 3 A g^{-1}	[17]
Birnessite MnO_2	0.25 M $ZnSO_4$ +0.75 M Na_2SO_4	305 mAh g^{-1} at 308 mA g^{-1}	45.9% retained at 3.08 A g^{-1}	53% retained after 1000 cycles at 3.08 A g^{-1}	[18]
λ-MnO_2	1 M $ZnSO_4$	442.6 mAh g^{-1}	7.6% retained	-	[19]

		at 13.6 mA g^{-1}	at 0.408 A g^{-1}		
ε-MnO_2 on carbon fiber	2 M $ZnSO_4$ +0.2 M $MnSO_4$	290 mAh g^{-1} at 90 mA g^{-1}	58.6% retained at 1.95 A g^{-1}	99.3% retained after 10000 cycles at 1.95 A g^{-1}	[20]
$Li_xV_2O_5$·nH_2O	2 M $ZnSO_4$	470 mA h g-1 at 0.5 A g^{-1}	36.2% retained at 10 A g^{-1}	100% retained after 1000 cycles at 10 A g^{-1}	[21]
$Zn_{0.25}V_2O_5$•n H_2O	1 M $ZnSO_4$	282 mAh g^{-1} at 300 mA g^{-1}	93% retained at 2.4 A g^{-1}	80% retained after 1000 cycles at 2.4 A g^{-1}	[22]
$Ca_{0.25}V_2O_5$	1 M $ZnSO_4$	340 mAh g^{-1} at 0.2 C	21.2% retained at 80 C	64% retained after 5000 cycles at 80 C	[23]
$Na_{0.33}V_2O_5$	3 M $Zn(CF_3SO_3)_2$	373 mAh g^{-1} at 200 mA g-1	25.8% retained at 2 A g^{-1}	93% retained after 1000 cycles at 1 A g^{-1}	[24]

References

[1] W. Chen, G. Li, A. Pei, Y. Li, L. Liao, H. Wang, J. Wan, Z. Liang, G. Chen, H. Zhang, J. Wang, Y. Cui, A manganese–hydrogen battery with potential for grid-scale energy storage, Nature Energy, 3 (2018) 428-435.

[2] G. Fang, C. Zhu, M. Chen, J. Zhou, B. Tang, X. Cao, X. Zheng, A. Pan, S. Liang, Suppressing Manganese Dissolution in Potassium Manganate with Rich Oxygen Defects Engaged High-Energy-Density and Durable Aqueous Zinc-Ion Battery, Advanced Functional Materials, 29 (2019) 1808375.

[3] V. Augustyn, P. Simon, B. Dunn, Pseudocapacitive oxide materials for high-rate electrochemical energy storage, Energy & Environmental Science, 7 (2014) 1597-1614.

[4] D. Chao, C. Zhu, P. Yang, X. Xia, J. Liu, J. Wang, X. Fan, S.V. Savilov, J. Lin, H.J. Fan, Z.X. Shen, Array of nanosheets render ultrafast and high-capacity Na-ion storage by tunable pseudocapacitance, Nature Communications, 7 (2016) 12122.

[5] D. Chao, P. Liang, Z. Chen, L. Bai, H. Shen, X. Liu, X. Xia, Y. Zhao, S.V. Savilov, J. Lin, Z.X. Shen, Pseudocapacitive Na-Ion Storage Boosts High Rate and Areal Capacity of Self-Branched 2D Layered Metal Chalcogenide Nanoarrays, ACS Nano, 10 (2016) 10211-10219.

[6] Y. Zeng, X. Zhang, Y. Meng, M. Yu, J. Yi, Y. Wu, X. Lu, Y. Tong, Achieving Ultrahigh Energy Density and Long Durability in a Flexible Rechargeable Quasi-Solid-State Zn–MnO2 Battery, Advanced Materials, 29 (2017) 1700274.

[7] T. Xiong, Z.G. Yu, H. Wu, Y. Du, Q. Xie, J. Chen, Y.-W. Zhang, S.J. Pennycook,

W.S.V. Lee, J. Xue, Defect Engineering of Oxygen-Deficient Manganese Oxide to Achieve High-Performing Aqueous Zinc Ion Battery, Advanced Energy Materials, 9 (2019) 1803815.

[8] M.H. Alfaruqi, J. Gim, S. Kim, J. Song, D.T. Pham, J. Jo, Z. Xiu, V. Mathew, J. Kim, A layered δ-MnO2 nanoflake cathode with high zinc-storage capacities for eco-friendly battery applications, Electrochemistry Communications, 60 (2015) 121-125.

[9] M.H. Alfaruqi, J. Gim, S. Kim, J. Song, J. Jo, S. Kim, V. Mathew, J. Kim, Enhanced reversible divalent zinc storage in a structurally stable α-MnO2 nanorod electrode, Journal of Power Sources, 288 (2015) 320-327.

[10] N. Zhang, F. Cheng, J. Liu, L. Wang, X. Long, X. Liu, F. Li, J. Chen, Rechargeable aqueous zinc-manganese dioxide batteries with high energy and power densities, Nature Communications, 8 (2017) 405.

[11] J. Huang, Z. Wang, M. Hou, X. Dong, Y. Liu, Y. Wang, Y. Xia, Polyaniline-intercalated manganese dioxide nanolayers as a high-performance cathode material for an aqueous zinc-ion battery, Nature Communications, 9 (2018) 2906.

[12] H. Zhang, J. Wang, Q. Liu, W. He, Z. Lai, X. Zhang, M. Yu, Y. Tong, X. Lu, Extracting oxygen anions from ZnMn2O4: Robust cathode for flexible all-solid-state Zn-ion batteries, Energy Storage Materials, 21 (2019) 154-161.

[13] M.H. Alfaruqi, S. Islam, D.Y. Putro, V. Mathew, S. Kim, J. Jo, S. Kim, Y.-K. Sun, K. Kim, J. Kim, Structural transformation and electrochemical study of layered MnO2 in rechargeable aqueous zinc-ion battery, Electrochimica Acta, 276 (2018) 1-11.

[14] Y. Fu, Q. Wei, G. Zhang, X. Wang, J. Zhang, Y. Hu, D. Wang, L. Zuin, T. Zhou, Y. Wu, S. Sun, High-Performance Reversible Aqueous Zn-Ion Battery Based on Porous MnOx Nanorods Coated by MOF-Derived N-Doped Carbon, Advanced Energy Materials, 8 (2018) 1801445.

[15] Y. Huang, J. Liu, Q. Huang, Z. Zheng, P. Hiralal, F. Zheng, D. Ozgit, S. Su, S. Chen, P.-H. Tan, S. Zhang, H. Zhou, Flexible high energy density zinc-ion batteries enabled by binder-free MnO2/reduced graphene oxide electrode, npj Flexible Electronics, 2 (2018) 21.

[16] W. Qiu, Y. Li, A. You, Z. Zhang, G. Li, X. Lu, Y. Tong, High-performance flexible quasi-solid-state Zn–MnO2 battery based on MnO2 nanorod arrays coated 3D porous nitrogen-doped carbon cloth, Journal of Materials Chemistry A, 5 (2017) 14838-14846.

[17] B. Wu, G. Zhang, M. Yan, T. Xiong, P. He, L. He, X. Xu, L. Mai, Graphene Scroll-Coated α-MnO2 Nanowires as High-Performance Cathode Materials for Aqueous Zn-Ion Battery, Small, 14 (2018) 1703850.

[18] J.S. Ko, M.B. Sassin, J.F. Parker, D.R. Rolison, Jeffrey W. Long, Combining battery-like and pseudocapacitive charge storage in 3D MnOx@carbon electrode architectures for zinc-ion cells, Sustainable Energy & Fuels, 2 (2018) 626-636.

[19] C. Yuan, Y. Zhang, Y. Pan, X. Liu, G. Wang, D. Cao, Investigation of the intercalation of polyvalent cations (Mg2+, Zn2+) into λ-MnO2 for rechargeable aqueous battery, Electrochimica Acta, 116 (2014) 404-412.

[20] W. Sun, F. Wang, S. Hou, C. Yang, X. Fan, Z. Ma, T. Gao, F. Han, R. Hu, M.

Zhu, C. Wang, Zn/MnO2 Battery Chemistry With H+ and Zn2+ Coinsertion, Journal of the American Chemical Society, 139 (2017) 9775-9778.

[21] Y. Yang, Y. Tang, G. Fang, L. Shan, J. Guo, W. Zhang, C. Wang, L. Wang, J. Zhou, S. Liang, Li+ intercalated V2O5·nH2O with enlarged layer spacing and fast ion diffusion as an aqueous zinc-ion battery cathode, Energy & Environmental Science, 11 (2018) 3157-3162.

[22] D. Kundu, B.D. Adams, V. Duffort, S.H. Vajargah, L.F. Nazar, A high-capacity and long-life aqueous rechargeable zinc battery using a metal oxide intercalation cathode, Nature Energy, 1 (2016) 16119.

[23] C. Xia, J. Guo, P. Li, X. Zhang, H.N. Alshareef, Highly Stable Aqueous Zinc-Ion Storage Using a Layered Calcium Vanadium Oxide Bronze Cathode, Angewandte Chemie International Edition, 57 (2018) 3943-3948.

[24] P. He, G. Zhang, X. Liao, M. Yan, X. Xu, Q. An, J. Liu, L. Mai, Sodium Ion Stabilized Vanadium Oxide Nanowire Cathode for High-Performance Zinc-Ion Batteries, Advanced Energy Materials, 8 (2018) 1702463.